Concentric-flow electrokinetic injector enables serial crystallography of ribosome and photosystem II

Raymond G Sierra[1], Cornelius Gati[2], Hartawan Laksmono[1], E Han Dao[1], Sheraz Gul[3], Franklin Fuller[3], Jan Kern[3,4], Ruchira Chatterjee[3], Mohamed Ibrahim[5], Aaron S Brewster[3], Iris D Young[3], Tara Michels-Clark[3], Andrew Aquila[4], Mengning Liang[4], Mark S Hunter[4], Jason E Koglin[4], Sébastien Boutet[4], Elia A Junco[4], Brandon Hayes[4], Michael J Bogan[1], Christina Y Hampton[1], Elisabetta V Puglisi[6], Nicholas K Sauter[3], Claudiu A Stan[1], Athina Zouni[5], Junko Yano[3], Vittal K Yachandra[3], S Michael Soltis[7], Joseph D Puglisi[6] & Hasan DeMirci[1,7]

We describe a concentric-flow electrokinetic injector for efficiently delivering microcrystals for serial femtosecond X-ray crystallography analysis that enables studies of challenging biological systems in their unadulterated mother liquor. We used the injector to analyze microcrystals of *Geobacillus stearothermophilus* thermolysin (2.2-Å structure), *Thermosynechococcus elongatus* photosystem II (<3-Å diffraction) and *Thermus thermophilus* small ribosomal subunit bound to the antibiotic paromomycin at ambient temperature (3.4-Å structure).

© 2016 Nature America, Inc. All rights reserved.

The development of serial femtosecond X-ray crystallography[1] (SFX) with X-ray free-electron lasers (XFELs) is pushing the frontiers of structural biology[2,3]. In addition to enabling the structural determination of challenging new targets, SFX can be used at ambient temperature to re-examine structures of biological macromolecules and complexes previously determined at cryogenic temperatures using synchrotron radiation[4].

New methods for SFX are usually validated using protein crystal standards[5,6]. Success with these standards does not translate directly to more difficult systems such as ribosomes and photosystem II (PSII). Sample delivery to the XFEL beam is not trivial, as it requires that a stream of microcrystals intersect with the femtosecond pulses of an XFEL. An ideal SFX injection method would require minimal alterations to the crystals' growth medium (mother liquor), would consume minimal sample and would maximize the sample–to–X-ray pulse interaction (hit rate). Liquid injectors currently offer the best hit rates by using the full repetition rate of XFELs, in contrast to current fixed-target approaches[7], but they have drawbacks. The gas dynamic virtual nozzle[8] focuses a liquid jet using a gas stream. This device provides robust sample delivery but consumes samples somewhat inefficiently, as a large volume of sample flows unused between XFEL pulses, and it is generally incompatible with high-viscosity media. The microfluidic electrokinetic sample holder[9] (MESH) operates at low flow rates by applying voltage rather than pressure. Although operation of the MESH at atmospheric conditions is trivial, the low vacuum pressures of existing XFEL experiment chambers cause the fluid at the meniscus to evaporate quickly. Consequently, freezing and precipitation of solutes occurs, causing jet failures and preventing data collection. A typical workaround is to place an additive in the crystallization sample. Lipidic cubic phase[10] (LCP) and grease-matrix injectors[11] are more efficient because of the high viscosity of their carrier media, which enables slow extrusion of the samples; however, these media have high background scattering and are not compatible with all protein crystals. The SFX field still is in need of more robust injection methods for delivering soluble protein crystals in their native mother liquor with minimal sample consumption.

We developed the concentric MESH injector (coMESH) to address this need. The coMESH uses an inner capillary to introduce crystalline samples, suspended in their native mother liquor, into the XFEL beam. An outer sheath (the 'sister liquor') prevents dehydration and freezing of the sample fluid after it is introduced to the vacuum chamber (**Fig. 1** and **Supplementary Figs. 1** and **2**). This concentric-flow design is an improvement on the prior MESH method and resolves its limitations (**Supplementary Table 1**). The coMESH can be made from off-the-shelf parts.

The coMESH improved the hit rate and the quality of data collected from PSII crystals compared with values obtained via single-capillary MESH (**Supplementary Figs. 3–5**). PSII crystallized under conditions with a high percentage of PEG 5000 (ref. 12), which caused the meniscus of the MESH to dehydrate quickly in vacuum. Large deposits of dried PEG 5000 accumulated at the tip of the injector and caused frequent jet failures, decreasing the amount of time available for data collection between blockages (**Supplementary Fig. 4c**). Use of the coMESH with coterminal capillaries eliminated freezing and drying issues and allowed for

[1]Stanford PULSE Institute, SLAC National Accelerator Laboratory, Menlo Park, California, USA. [2]Center for Free-Electron Laser Science, Deutsches Elektronen-Synchrotron, Hamburg, Germany. [3]Lawrence Berkeley National Laboratory, Berkeley, California, USA. [4]Linac Coherent Light Source, SLAC National Accelerator Laboratory, Menlo Park, California, USA. [5]Institute für Biologie, Humboldt University of Berlin, Berlin, Germany. [6]Department of Structural Biology, Stanford University School of Medicine, Stanford, California, USA. [7]Stanford Synchrotron Radiation Lightsource, SLAC National Accelerator Laboratory, Menlo Park, California, USA. Correspondence should be addressed to H.D. (hasan_demirci@stanford.edu) or R.G.S. (rsierra@stanford.edu).

RECEIVED 8 JULY; ACCEPTED 14 OCTOBER; PUBLISHED ONLINE 30 NOVEMBER 2015; DOI:10.1038/NMETH.3667

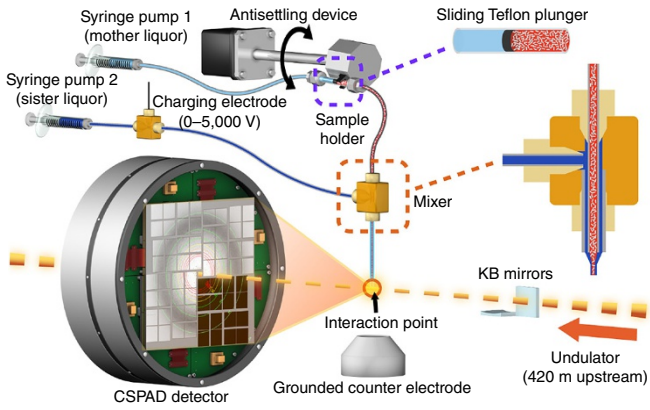

Figure 1 | The concentric-flow MESH injector setup at the CXI instrument of the LCLS. The liquid jet, containing microcrystals and their mother liquor (red), flows in the continuous inner capillary (100 µm × 160 µm × 1.5 m) (**Supplementary Fig. 3a**). The sister liquor (dark blue) is charged by a high-voltage power supply (0–5,000 V) for electrofocusing of the liquid jet. A mixer (indicated by the dashed orange square) joins the two capillaries concentrically (**Supplementary Fig. 2**). The sample reservoir contains a Teflon plunger (black band in upper right image) that separates the sample reservoir from the driving fluid (light blue). The reservoir is mounted on an antisettling device that rotates, at an angle, about the capillary axis to keep the protein crystals suspended homogeneously in the slurry. The liquid jet and the LCLS pulses interact at the point indicated by the orange circle ("interaction point"). The bottom right quadrant of the detector was nonfunctional during ribosome data collection (indicated by dark shading; active quadrants are shaded light gray). CSPAD, Cornell-SLAC pixel-array detector; KB, Kirkpatrick-Baez.

observation of diffraction beyond 3.0 Å (**Supplementary Fig. 5b**) with the Coherent X-ray Imaging (CXI) instrument of the Linac Coherent Light Source[13] (LCLS). Use of the coMESH permitted continuous data collection for 2–2.5 h, an improvement over mean data-collection times of 20–30 min between failures of the jet in the single-capillary MESH setup due to PEG buildup.

In a protein crystal screening experiment, we also determined the structure of a 30S ribosomal subunit–paromomycin complex to 3.4 Å at ambient temperature by SFX using coMESH sample delivery at the CXI instrument[13] (**Supplementary Table 2**). We observed substantial conformational shifts (**Fig. 2**) when we compared the ambient-temperature structure with a cryo-cooled synchrotron structure (3.35 Å; PDB ID 4DR2)[14]. Superposition of the cryo-cooled and ambient-temperature structures showed that the 'head' and 'beak' domains adopted slightly altered conformations (**Fig. 2**). A least-squares alignment of all 17,056 16S rRNA atoms in the two 30S structures showed an overall r.m.s. deviation of 0.488 Å. Interesting conformational differences (up to 3.6 Å) between the two structures were found at the 926–934 and 1,378–1,385 regions, which are part of helix 28 (h28) of the 16S rRNA (**Fig. 3**). Comparison of the two structures also showed differences in the H-bond network of paromomycin (**Fig. 3d**). In the cryo-cooled structure, the O23 atom of paromomycin engaged in a 2.85-Å H-bond with the N4 atom of the m5C1407 residue, compared to 3.4 Å at ambient temperature, suggesting a weakening of this particular interaction. Also, a 1.4-Å shift in the position of O23 introduced further changes in the conformation of paromomycin ring III (**Supplementary Table 3**). For example, in the new state, O23 protrudes out of the experimental F_o-F_c simple difference omit map (**Fig. 3c**).

In a previous protein crystal screening experiment, SFX data for 30S ribosomal subunit crystals were collected at the CXI instrument[15] using gas dynamic virtual nozzle injection; the crystals diffracted to 5.5 Å. In those data, 637 indexed hits were identified out of 1,074,902 diffraction patterns. More than 15 ml of sample was used during the 6-h beamtime. In comparison, 20,667 indexed hits were identified out of 44,106 patterns collected from 360 µl of sample consumed in 2 h of data collection to solve the 3.4-Å structure reported here.

Ribosomes are structurally dynamic and undergo local and large-scale conformational rearrangements during the individual steps of protein synthesis[16]. X-ray crystallography data for ribosomes and other large complexes are typically collected at cryogenic temperatures, as these crystals are extremely sensitive to radiation damage[17]. Cryo-cooling thus enables data collection but may mask useful details about local and global conformational dynamics and allostery. Structures of ribosomes obtained at temperatures closer to the physiological range can reveal alternative conformations and structural dynamics, such as the alternative conformation of h28 (hinge 1) identified here. Some of these structural variations may be precisely linked to function[18]. Hinge 1 of the 30S subunit[18] confers the remarkable plasticity of the head domain and allows the head of the ribosome to move freely between functional states during translation. Here the

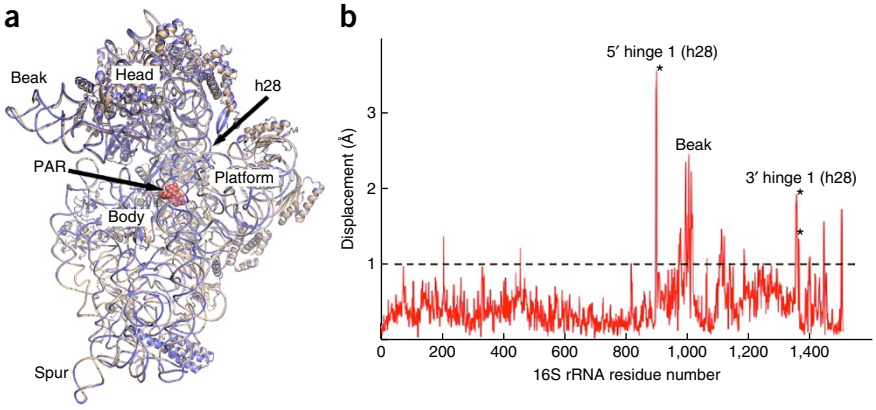

Figure 2 | Comparison of cryo-cooled and ambient-temperature *T. thermophilus* 30S-paromomycin complex structures. (**a**) The ambient-temperature structure (light brown) is superposed on the cryo-cooled structure[14] (blue). The positions of the major 30S domains are indicated. The locations of paromomycin (PAR) (salmon-colored spheres) and 16S rRNA h28 in the ambient-temperature structure are shown by arrows. All X-ray crystal-structure figures were produced with PyMOL (http://www.schrodinger.com/pymol). (**b**) Pairwise distances between 16S rRNA phosphate atoms plotted after alignment of all phosphate atoms of bases 5–1,532 between the ambient and cryo-30S structures. Major shifts of more than 1 Å are visualized as sharp spikes and were observed at and around the hinge 1 region of h28 (indicated by asterisks) and the beak domain. The dashed line denotes the 1-Å displacement threshold.

© 2016 Nature America, Inc. All rights reserved.

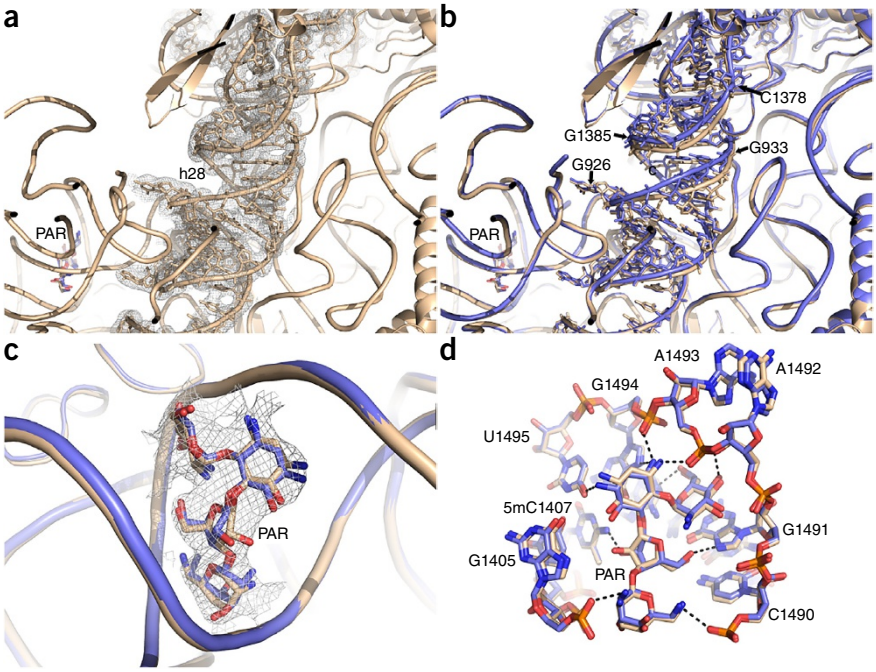

Figure 3 | Structural changes were observed in h28 and in paromomycin binding at ambient temperature. (**a**) Final unbiased F_o-F_c simple omit electron-density map of h28 contoured at the 3σ level, colored in gray and shown at 3 Å. The locations of paromomycin and h28 are indicated. (**b**) Superposition of the cryo- and ambient-temperature structures showing displacement of the h28 backbone. This view illustrates the shifts in positions 926–933 and 1,375–1,385. (**c**) Final unbiased F_o-F_c simple omit difference electron-density map of the paromomycin-binding site contoured at the 3σ level, colored in gray and shown at 3 Å. (**d**) Comparison of the contacts between cryo- and ambient-temperature 16S rRNA helix 44 and paromomycin. The bending of the paromomycin molecule is visible with an altered H-bonding network; the view in **c** is rotated nearly 180° around the vertical axis. Color schemes are the same as in **Figure 2a**.

h28 phosphate backbone exhibited shifts of up to 3.6 Å at ambient temperature (**Figs. 2b** and **3b**), in contrast to the more rigid and dehydrated cryo-cooled structure. These differences can have major implications with respect to binding of paromomycin to the ribosome and the effects of antibiotic binding to ribosomes in general, which are relevant for the structure-based drug design of new antibiotics. The same motivation may also hold for many other enzymatic systems such as PSII, a membrane metalloprotein complex that so far has been studied at high resolution only in cryogenically trapped states[19] but which functions at ambient temperatures.

We also solved a 2.2-Å structure of thermolysin (**Supplementary Fig. 6**) using the coMESH in an alternate configuration (**Supplementary Fig. 3d**).

The capillaries of the coMESH design, which have an inner diameter of 100 µm, allow unfiltered crystals up to 40 µm in size to flow without clogging. Other setups typically use capillaries with inner diameters of 40–75 µm, keeping flow rates between 1 and 3 µl min^{-1}. In comparison, LCP injection[10] flows at hundreds of nanoliters per minute but requires either crystallization in LCP or sample churning into the viscous LCP. For membrane proteins such as G protein–coupled receptors, LCP injection is an ideal technique; however, it is unclear whether soluble proteins can be crystallized in or mixed into the LCP matrix easily. Similarly, greases, oils and gels may be ideal for certain crystals but not others[11]. The coMESH permits protein crystals to flow in their established mother liquor and coflow with an appropriate sister liquor (**Supplementary Table 1**).

We found that a key limitation of the single-capillary MESH approach was the need to dope the mother liquor such that the final crystal suspension would not freeze *in vacuo*. Finding an additive that permits sample injection while maintaining the integrity of the crystals is not always feasible. In the coMESH, however, the capillaries are placed coterminally such that the sister liquor protects the mother liquor from vacuum effects with minimal mixing before the sample reaches the incident XFEL probe[20] (**Fig. 1**). The prevention of freezing, dehydration and precipitation of the sample slurry *in vacuo* maximizes the time available for data collection.

In conclusion, we report a concentric-flow liquid injection technique for SFX. We anticipate that the coMESH will enable the use of a wider range of soluble protein crystal slurries in SFX. Use of the sister liquor addresses the MESH's inability to tolerate vacuum injection without an appropriately modified mother liquor that maintains the integrity of the suspended crystals. The coMESH arrives at an exciting time for the structural biology community when cryo–electron microscopy and cryo-crystallography structures of complexes can be combined with SFX for studies of biological macromolecules at near-physiological temperatures. In the future, the concentric geometry of the coMESH could easily be modified to recess the inner capillary and create the basis of a mixing apparatus for exploring structural intermediates over time[20]. The sister liquor could be doped with a reactant to initiate structural changes for time-resolved mix-and-probe experiments at XFELs, such as mixing of ribosomes with antibiotics, substrates and translation factors. Time-resolved SFX could move beyond photo-excited systems to include a vast mix-probe regime. These future mix-probe studies would allow for examination of the dynamic details of binding events at hitherto-inaccessible timescales, temperatures and resolution.

METHODS

Methods and any associated references are available in the online version of the paper.

Accession codes. Coordinates and structure factors of the 30S-paromomycin complex and thermolysin have been deposited in the RCSB Protein Data Bank under accession codes 5BR8 and 5DLH, respectively.

Note: Any Supplementary Information and Source Data files are available in the online version of the paper.

© 2016 Nature America, Inc. All rights reserved.

ACKNOWLEDGMENTS
Portions of this research were carried out at the LCLS at the SLAC National Accelerator Laboratory. The LCLS is supported by the US Department of Energy (DOE), Office of Science, Office of Basic Energy Sciences (OBES), under contract DE-AC02-76SF00515. This research used resources of the National Energy Research Scientific Computing Center, a DOE Office of Science User Facility supported by the Office of Science, DOE, under contract DE-AC02-05CH11231. Part of the sample-injector mechanical system used at LCLS for this research was funded by the US National Institutes of Health (NIH) (P41GM103393, formerly P41RR001209). J.Y. and V.K.Y. are supported by the Office of Science, OBES, Chemical Sciences, Geosciences, and Biosciences (CSGB) of the DOE under contract DE-AC02-05CH11231 for X-ray methodology and instrumentation. The LCLS is acknowledged for beam time access under experiments cxig7014, cxib6714 and cxig3614. E.H.D., H.L., R.G.S., M.J.B., C.Y.H., C.A.S. and H.D. acknowledge the support of the OBES through the AMOS program within the CSGB and of the DOE through the SLAC Laboratory Directed Research and Development Program. N.K.S. acknowledges an LBNL Laboratory Directed Research and Development award under contract DE-AC02-05CH11231. E.H.D. acknowledges financial support from the Stanford University Dean of Research. H.D., S.M.S. and J.D.P. acknowledge support from the joint Stanford ChEM-H and SLAC National Accelerator Laboratory seed grant program. This work is supported by NIH grants GM51266 (to J.D.P.), GM082545 (to E.V.P.), GM055302 (to V.K.Y.), GM110501 (to J.Y.), GM095887 and GM102520 (to N.K.S.); the DFG–Cluster of Excellence "UniCat" coordinated by the Technische Universitaet at Berlin and Sfb1078, TP A5 (to A.Z. and M.I.); and Human Frontiers Science Project awards RGP0005/2011 (to H.L.) and RGP0063/2013 310 (to J.Y. and A.Z.). C.G. kindly thanks the PIER Helmholtz Graduate School, as well as the Helmholtz Association for financial support. H.D. acknowledges valuable discussions with A. Takeuchi, K. Dursuncan and E. Satunaz. We thank M. West for support in designing and machining the injector load lock setup and G. Stewart for excellent technical assistance with creating the graphics for **Figure 1**.

AUTHOR CONTRIBUTIONS
H.D. and R.G.S. designed and coordinated the project. R.G.S., H.L., H.D., C.A.S., C.Y.H., S.G., F.F. and M.J.B. developed the coMESH injection method. C.G. executed the ribosome data reduction. H.D. refined ribosome and thermolysin structures. N.K.S., A.S.B., I.D.Y. and T.M.-C. processed PSII and thermolysin diffraction data. H.D., E.H.D., B.H., R.C., I.D.Y., M.I., J.K. and A.Z. prepared samples. R.G.S., H.D., H.L., C.A.S., E.H.D., S.G., F.F., J.K., R.C., M.I., A.A., M.L., M.S.H., J.E.K., S.B., E.A.J., J.Y. and V.K.Y. carried out the experiment. H.D., C.G., R.G.S., E.V.P., J.K., J.Y., V.K.Y., S.M.S. and J.D.P. analyzed data. H.D., R.G.S., E.H.D., C.G., H.L., C.A.S. and J.K. prepared the manuscript with input from all other coauthors.

COMPETING FINANCIAL INTERESTS
The authors declare competing financial interests: details are available in the online version of the paper.

Reprints and permissions information is available online at http://www.nature.com/reprints/index.html.

1. Neutze, R., Wouts, R., van der Spoel, D., Weckert, E. & Hajdu, J. *Nature* **406**, 752–757 (2000).
2. Tenboer, J. *et al. Science* **346**, 1242–1246 (2014).
3. Chapman, H.N. *et al. Nature* **470**, 73–77 (2011).
4. Liu, W. *et al. Science* **342**, 1521–1524 (2013).
5. Boutet, S. *et al. Science* **337**, 362–364 (2012).
6. Hattne, J. *et al. Nat. Methods* **11**, 545–548 (2014).
7. Hunter, M.S. *et al. Sci. Rep.* **4**, 6026 (2014).
8. DePonte, D.P. *et al. Micron* **40**, 507–509 (2009).
9. Sierra, R.G. *et al. Acta Crystallogr. D Biol. Crystallogr.* **68**, 1584–1587 (2012).
10. Weierstall, U. *et al. Nat. Commun.* **5**, 3309 (2014).
11. Sugahara, M. *et al. Nat. Methods* **12**, 61–63 (2015).
12. Hellmich, J. *et al. Structure* **22**, 1607–1615 (2014).
13. Liang, M. *et al. J. Synchrotron Radiat.* **22**, 514–519 (2015).
14. DeMirci, H. *et al. Nat. Commun.* **4**, 1355 (2013).
15. DeMirci, H. *et al. Acta Crystallogr. Sect. F Struct. Biol. Cryst. Commun.* **69**, 1066–1069 (2013).
16. Petrov, A., Chen, J., O'Leary, S., Tsai, A. & Puglisi, J.D. *Cold Spring Harb. Perspect. Biol.* **4**, a011551 (2012).
17. Warkentin, M., Hopkins, J.B., Haber, J.B., Blaha, G. & Thorne, R.E. *Acta Crystallogr. D Biol. Crystallogr.* **70**, 2890–2896 (2014).
18. Mohan, S., Donohue, J.P. & Noller, H.F. *Proc. Natl. Acad. Sci. USA* **111**, 13325–13330 (2014).
19. Suga, M. *et al. Nature* **517**, 99–103 (2015).
20. Wilson, D.J. & Konermann, L. *Anal. Chem.* **75**, 6408–6414 (2003).

© 2016 Nature America, Inc. All rights reserved.
npg

ONLINE METHODS

Preparation and crystallization of 30S ribosomal subunits. 30S ribosomal subunits from *T. thermophilus* HB8 (ATCC 27634)[21] were prepared as previously described[22,23]. Purified 30S ribosomal subunits were crystallized at 4 °C via the hanging-drop method using a mother liquor solution containing 17% (vol/vol) 2-methyl-2, 4-pentanediol (MPD), 15 mM magnesium acetate, 200 mM potassium acetate, 75 mM ammonium acetate and 100 mM 2-(*N*-morpholino) ethanesulfonic acid (MES)-KOH, pH 6.5. Microcrystals 3–10 × 3–10 × 20–30 μm^3 in size were harvested in the same mother liquor composition, pooled (total volume of 800 µl loaded) and supplemented with 80 µM paromomycin for 48 h before data collection. The crystal concentration was approximately 10^{10}–10^{11} particles per milliliter based on light microscopy and nanoparticle-tracking analysis (NanoSight LM10-HS with corresponding Nanoparticle Tracking Analysis (NTA) software suite (Malvern Instruments, Malvern, UK)).

Preparation and crystallization of PSII crystals and solution. Crystals of *T. elongatus* PSII were grown as described previously[12]; a uniform crystal size of 5–15 µm was achieved by means of a seeding protocol[24]. The crystals were transferred to a final buffer of 35% (wt/vol) PEG 5000, 0.1 M ammonium sulfate, 0.1 M Tris, pH 7.5, before being loaded into a 250-µl volume Hamilton Gastight syringe for sample injection. PSII solution samples were prepared from purified dimeric PSII according to the procedure described previously[25]. The final solution was adjusted to a protein concentration of ~6.7 mM chlorophyll (70 mg/ml protein), a glycerol content of 40% (vol/vol) and a detergent (β-dodecyl maltoside) concentration of 0.015% (vol/vol).

Preparation of thermolysin crystals. Lyophilized thermolysin from *G. stearothermophilus*, purchased from Hampton Research (La Jolla, CA, USA), was resuspended in 0.05 M NaOH at a concentration of 25 mg/ml and crystallized as described previously[6,9,26] using PEG 2000 as a precipitant. Crystals had average dimensions of 3 µm × 5 µm and were transferred in a final buffer of 10% (wt/vol) PEG 2000, 38% (vol/vol) glycerol, 5 mM $CaCl_2$, 100 mM MES, pH 6.5, before injection.

coMESH construction. The central sample line was a continuous 100-µm inner diameter fused silica capillary with a 160-µm outer diameter and a length of 1.5 m (Polymicro, Phoenix, AZ, USA). This capillary directly connected the reservoir with the interaction region, passing through a vacuum feed-through and then through a microfluidic Interconnect Cross (C360-204, LabSmith, Livermore, CA, USA; a C360-203 Interconnect Tee may also be used with no need to plug the fourth channel) (**Supplementary Fig. 2**). Feeding the sample through an uninterrupted straight capillary without filters, unions or connections minimized the risk of sample clogs and leaks, which most often occur at flow-channel transitions. In addition, the large capillary inner diameter allowed the crystal slurry to flow in the system with no inline filtration or filters at the reservoir. The fitting at the top of the cross in **Supplementary Figure 2** was an adaptor fitting (T116-A360 as well as T116-100, LabSmith, Livermore, CA, USA) that compressed a 1/16-in. (1.6-mm) outer diameter, 0.007-in. (178-µm) inner diameter polymer (fluorinated ethylene propylene) tubing sleeve (F-238, Upchurch, Oak Harbor, WA, USA) onto the sample capillary. This connection method was necessary to properly seal the capillary to the cross. The sheath line at the bottom of **Supplementary Figure 2** was a short, 5-cm fused silica capillary with an outer diameter of 360 µm and an inner diameter of 180, 200 or 250 µm, depending on the desired flow rate of the sheath liquid possible with the driving pressure available. The length and inner diameter of this line were chosen so as to allow sufficient flow for the sheath line. This outer capillary was connected to the cross, and the sheath liquid was supplied from the third port of the cross (the right port in **Supplementary Fig. 2**) through compatible microfluidic tubing; we typically used silica capillaries with 360-µm outer diameters and 75- or 100-µm inner diameters, depending on the flow rate desired. For simplicity, the injector was designed to operate at relatively low backing pressures (up to a few atmospheres). To achieve a given flow rate of the liquids, the fluidic resistance of the lines was varied, typically by changing the inner diameter of the capillaries used in the injector. For this experiment, the sheath liquid line was connected to a syringe filled with the appropriate sister liquor driven by a syringe pump (PHD Ultra, 703006, Harvard Apparatus, Holliston, MA, USA). We electrically charged the sheath liquid to between 0 and 5,000 V using an in-line conductive charging union (M-572, Upchurch, Oak Harbor, WA, USA) connected to an SRS PS350 (Stanford Research Systems, Sunnyvale, CA, USA) high-voltage source.

The capillary assembly was loaded into the CXI 1 × 1 μm^2 focused beam chamber with a custom load lock system developed at Lawrence Berkeley National Laboratory (**Supplementary Figs. 7** and **8**). This load lock system allowed for fast changes and cleaning of the injector capillary without the need to vent the main chamber of the CXI instrument. A grounded, conical counter electrode with a 1-cm opening was placed approximately 5 mm below the capillary tip; the capillaries and opening of the cone were coaxial. The angle of the cone and its distance from the tip were set to enable a diffraction cone with a 45° half-angle. All capillaries were fed through vacuum flanges with 1/16-in. (1.6-mm) Swagelok bulkhead fittings using appropriately sized polymer sleeves. The sheath reservoir was a 1-ml Gastight Hamilton syringe with a polytetrafluoroethylene Luer tip (1001 TLL SYR, Hamilton, USA). The sample was supplied either from a 500-µl Hamilton gas-tight syringe (for PSII and thermolysin) using a syringe pump or from a custom 5-ml reservoir (for the ribosome crystals) developed at the Sample Environment Group at LCLS. This stainless steel reservoir contained a custom Teflon plug that separated the sample slurry from the pushing fluid (which was either water or the mother liquor to mitigate problems from any potential leaks) as shown schematically at the top of **Figure 1** and in **Supplementary Figure 8**. The backing fluid was driven by another syringe pump, but it could also be pressurized by compressed gas.

Operating the coMESH. Before the central sample line was connected, the sister liquor was loaded, flowed and electrically focused. Once a slightly stable jet was achieved, the central sample line was connected. Notably, the sister liquor never fully stabilized because the entrained air from the disconnected sample line continuously introduced bubbles. The central sample line had much less fluidic resistance than the outer line. Connecting it first with a vacuum-sensitive sample will cause immediate jet clogging and blockages; like the helium sheath line of the gas dynamic virtual

© 2016 Nature America, Inc. All rights reserved.

nozzle, the outer line should always be on while operating in vacuum. The sister liquor was set to flow at or near the flow rate of the mother liquor. If diffraction hits were not being observed, the sister liquor flow was reduced and/or the mother liquor flow was increased slowly to ensure that the jetting remained stable until the diffraction patterns appeared; it is possible that the flow rate of the sister liquor was too high compared with that of the mother liquor and was pinching off the inner flow of crystals.

Selecting a sister liquor. The main purposes of the sister liquor are to survive the vacuous environment (10^{-5} Torr) and protect the inner sample line from adverse vacuum effects. In the case of the coterminal coMESH, the compatibility between the sister liquor and the protein crystals was not considered because the fluid interaction occurred just before the sample was probed, allowing minimal time, if any, for the fluids to mix. The limiting constraints were typically the availability and viscosity of the fluid. For simplicity, the MPD-containing sister liquor described in **Supplementary Table 1** seems to be an ideal starting choice. The buffer proved to be quite reliable and survived the vacuum injection with minimal issues regarding dried sucrose or precipitates such as salt or PEG adhering to the capillary tip. The lower viscosity of the sister liquor allowed it to be pumped easily by a standard syringe pump through the more resistive cross manifold or concentric annular flow before the exit region of the capillary. Using a more viscous sister liquor, such as a glycerol–PEG 2000 mixture (**Supplementary Table 1**), can aid the mother liquor in certain instances, but the sister liquor might not flow fast enough to keep the mother liquor sufficiently quenched. Although this mixture worked to inject water (a difficult mother liquor to deliver at low flow rates because it freezes almost instantly when introduced to vacuum), it was easy for slight perturbations in the flow rates to cause the sample line to be exposed to vacuum and freeze. The high viscosity of the glycerol and PEG solution compared to the MPD solution made it difficult to increase the flow rate to ensure protection.

If MPD is not viable, the crystal's known cryo-protectant solution from standard synchrotron studies is another possibility. Oils might not be ideal for vacuum injection or sister liquor, as outgassing of the oil might not be tolerated by the sensitive in-vacuum optics in the experiment. More important, the oil will probably limit the charging ability of the sister liquor, which will hinder the focusing of the liquid jet. The novelty of the sister liquor is that properties of the fluid can be modified with minimal concern for the integrity of the crystal in the central line. For example, if a mother liquor with high-molarity salt is causing rapid dehydration in vacuum and the formation of data-compromising salt crystals, the sister liquor can be formulated with a low salt concentration (e.g., millimolar concentrations in the hundreds), some cryo-protectant and a pH buffer to aid in the injection with the coMESH.

If a high-viscosity sister liquor is required but cannot easily flow fast enough to protect the mother liquor, then changes can be made to the coMESH capillaries, such as shortening lengths and increasing diameters where possible. Also, instead of a syringe pump, HPLC or a high-pressure reservoir can be employed. In the current design, the greatest flow restrictions may be introduced by the off-the-shelf components, such as the inner diameter of the Labsmith cross or tee (250 µm) or the largest inner diameter for capillary with a 360-µm outer diameter; the maximum tolerable pressure is also limited to approximately 1,000 psi.

Sample injection. *Improved PSII injection in new mother liquor.* Previous time-resolved PSII experiments[26–28] carried out at LCLS relied on the single-capillary MESH injector. In previous LCLS solution spectroscopy experiments, the 70-mg/ml protein solution was supplemented with 1.0–1.4 M sucrose to prevent freezing. In SFX experiments, a prior crystallization condition of 10% (wt/vol) PEG 2000 was supplemented with 30% (vol/vol) glycerol to prevent freezing in vacuum and to reduce sample consumption during injection. Data up to 4.5-Å resolution were collected during these earlier experiments[26], but higher resolution for this sample was desired for improved observation of subtle time-dependent structural changes of the manganese metal center (Mn_4CaO_5) in its photodriven catalytic cycle. An improved crystallization condition yielding higher-quality PSII crystals contained a high percentage of PEG 5000 (ref. 12) (30–35% wt/vol), which caused the meniscus of the MESH to dehydrate quickly in vacuum and fail. These failure modes occurred frequently and limited the data-collection time (**Supplementary Fig. 4c**). The coMESH successfully injected the new mother liquor into vacuum by protecting it with the sister liquor (**Supplementary Table 1** and **Supplementary Fig. 3b**,**c**), thus eliminating the sudden failures caused by dried PEG 5000 at the meniscus. **Supplementary Table 1** lists several representative buffer compositions in which the original, single-capillary MESH configuration failed *in vacuo* but jetted properly with the new coMESH configurations. **Supplementary Figure 5** compares composite maximum images of two representative 9-min runs of PSII crystal suspensions using the two different coMESH injector setups at the CXI instrument[13] of the LCLS. The single-capillary MESH setup, used previously, required the addition of 35–40% ethylene glycol into the improved mother liquor, whereas the coMESH setup eliminated the need for ethylene glycol. The coMESH with a protruded inner capillary was used for thermolysin crystal suspensions (**Supplementary Fig. 3d**) and allowed collection of sufficient diffraction data for obtaining the structure (**Supplementary Fig. 6**). Tests with PSII crystal suspension in this protruded capillary geometry gave no indication of powder rings from dried PEG 5000 (**Supplementary Fig. 5a**), but there was still indication of freezing of the carrier liquid. In contrast, when we used the coMESH with coterminal capillaries (**Supplementary Fig. 5b**), freezing and drying problems were eliminated, and we observed diffraction beyond 3.0 Å. This decrease in jet failures resulted in continuous run times of 2–2.5 h, an improvement over mean run times of 20–30 min between blockages of the jet in the single-capillary MESH setup.

coMESH for ribosome crystals. The sample reservoir was loaded with 30S ribosome crystal slurry in mother liquor, described above. The sister liquor was identical to the mother liquor in that the original substituent concentrations remained constant, with the exception of a higher MPD concentration of 34% (vol/vol). The sample capillary was a fused silica capillary with 100-µm inner diameter × 160-µm outer diameter × 1.5-m length. The sheath flow capillary was a fused silica capillary with 75-µm inner diameter × 360-µm outer diameter × 1-m length. The outer concentric capillary was a tapered silica capillary with 200-µm inner diameter × 360-µm outer diameter × 5-cm length. The tips of the inner and outer capillaries were located at the same position. The taper of the outer capillary minimized the surface on which debris could build up after X-ray interaction with the sample but is not necessary for operation. The applied voltage on the sheath liquid

© 2016 Nature America, Inc. All rights reserved.

doi:10.1038/nmeth.3667

was typically 3,000 V, and the counter electrode was grounded. The sample ran typically between 0.75 and 3 μl/min, and the sheath flow rate typically matched or was slightly faster than the sample flow rate.

For the study of 30S ribosomal subunit crystals, the inner sample line contained unfiltered crystals in their native mother liquor containing 17% (vol/vol) MPD. The size distribution of the 30S crystals was uniform (3–10 × 3–10 × 20–30 μm^3) because of their controlled slower growth at 4 °C (ref. 22). Occasional larger 30S crystals were removed by repeated gentle differential settling without centrifugation and discarded. The outer sister liquor was the same buffer, with no crystals, as the mother liquor in that the original substituent concentrations remained constant, but the MPD concentration was increased to 34% (vol/vol) to aid in vacuum injection. The coMESH injector allowed us to successfully deliver 30S ribosomal subunit crystals (**Supplementary Fig. 3a**) and collect sufficient data to solve a complete ambient-temperature SFX structure, which was previously not attainable at an XFEL[15].

coMESH for PSII crystals. A 250-μl Gastight Hamilton glass syringe was loaded with PSII protein crystals in mother liquor, described above. The sister liquor was 50% (vol/vol) ethylene glycol, 50 mM Tris, pH 7.5, and 50 mM ammonium sulfate. The sample capillary was a fused silica capillary with 100-μm inner diameter × 160-μm outer diameter × 1.5-m length. The sheath flow capillary was a fused silica capillary with 75-μm inner diameter × 360-μm outer diameter × 1-m length. The outer concentric capillary was a tapered fused silica capillary with 200-μm inner diameter × 360-μm outer diameter × 5-cm length. The tips of the inner and outer capillaries were located at the same position. The sample was charged at the needle of the syringe with applied voltages of typically 7,000 V (PS365, Stanford Research Systems, Sunnyvale, CA, USA), and the counter electrode was grounded. The sample ran typically at flow rates between 0.75 and 3 μl/min, and the sheath flow rate matched or was faster than the sample flow rate to ensure proper isolation of the inner flow. For comparison, microcrystal suspensions were also run using the single-capillary MESH setup.

Protruded coMESH for PSII solution and crystals and thermolysin crystals. The solution X-ray emission spectroscopy experiments performed in vacuum could not handle the increased background noise from the thick (on the order of 10 μm) outer layer of sister liquor, but vacuum protection was still needed. We addressed this problem by slightly modifying the injector geometry, which was similar to that in the PSII setup described above. The exception was that the sample capillary protruded 1 mm beyond the tip of the outer capillary. In the case of thermolysin, the sister liquor was 50% (vol/vol) ethylene glycol, 100 mM MES, pH 6.5, and 5 mM $CaCl_2$. The sheath line had a smaller inner diameter of 30 μm to increase the fluidic resistance. Once the sheath line was primed with the sister liquor, the line was capped off and the liquor was allowed only to slowly trickle into vacuum, rather than having a driven flow. The voltage was applied on the sample line using a metal charging union.

Data collection and analysis. *Diffraction data collection of 30S ribosomal subunit microcrystals.* The SFX experiments with 30S ribosome microcrystals were carried out at the LCLS beam time ID CXIG7014 at the SLAC National Accelerator Laboratory (Menlo Park, CA). The LCLS X-ray beam with a pulse duration of 50 fs was focused using X-ray optics in a Kirkpatrick-Baez geometry to a beam size of 1.3 × 1.3 μm^2 full-width at half-maximum (FWHM) at a pulse energy of 2.9 mJ, a photon energy of 9.5 keV (1.29 Å) and a repetition rate of 120 Hz.

A total of 866,358 detector frames were collected with the Cornell-SLAC pixel-array detector[29] (CSPAD), corresponding to 120 min of data collection. The total beam time needed for this data set was 144 min, which shows the efficiency of this injector system, as owing to the lack of blockages no dead time was accumulated. Individual diffraction-pattern hits were defined as frames containing more than 30 Bragg peaks with a minimum signal-to-noise ratio greater than 4.5, which yielded a total of 44,106 images corresponding to an average hit rate of 5.1%. The detector distance was set at 223 mm, with an achievable resolution of 3.08 Å at the edge of the detector (2.6 Å in the corner). In this experiment, the fourth quadrant of the CSPAD detector was damaged and did not collect data.

After the detection of hits and the conversion of individual diffraction patterns to the HDF5 format, the software suite CrystFEL[30] (version 0.5.4, git ID 0477328) was used for crystallographic analysis. The peak location information from CHEETAH[31] was used for the indexing of individual, randomly oriented crystal diffraction patterns using fast Fourier transform–based indexing approaches. The detector geometry was refined using an automated algorithm to match found and predicted peaks to subpixel accuracy[32]. The integration step was performed using a built-in Monte Carlo algorithm[33,34] to estimate accurate structure factors from thousands of individually measured Bragg peaks. After the application of a per-pattern resolution cutoff, frames that did not match to an initial merged data set with a Pearson correlation coefficient of <0.4 were excluded from the final data set. The final set of indexed patterns, containing 20,667 frames (47% indexing rate), was merged into a final data set (overall $CC^* = 0.9822$; 3.4-Å cutoff) for further analysis ($P4_12_12$, unit cell: a = b = 401.3 Å, c = 176.4 Å; $\alpha = \beta = \gamma = 90°$). The final resolution cutoff was estimated as 3.4 Å using a combination of CC^*[35] and other refinement parameters. The final data set had an overall $R_{split} = 29.42\%$ and $CC^* = 0.70$ in the highest resolution shell.

Diffraction-data collection for PSII and thermolysin microcrystals. The SFX experiments with PSII and thermolysin microcrystals were carried out at the LCLS (beam time ID CXIG3614) at SLAC. The LCLS X-ray beam with a pulse duration of 50 fs was focused using X-ray optics in a Kirkpatrick-Baez geometry to a beam size of 1.3 × 1.3 μm^2 FWHM at a pulse energy of 0.9 mJ, using a photon energy of 7.1 keV (1.74 Å) and a repetition rate of 120 Hz. Diffraction data were analyzed using the cctbx.xfel software package[6,36]. We generated maximum-intensity composite images by adding all indexable diffraction patterns of one run (about 9 min of measurement time). For thermolysin, 153,943 CSPAD images were recorded during 21.5 min of data collection. Frames containing at least 16 Bragg peaks with a minimum analog-to-digital value of 450 and a total size of at least 4 pixels were considered hits, giving a total of 71,519 frames and a 46.5% hit rate. The detector distance was set at 119 mm, with an achievable resolution of 2.7 Å at the edge of the detector (2.2 Å in the corner). We indexed 38,222 hits in cctbx.xfel using fast Fourier transform–based indexing approaches (53.4% indexing rate). The detector geometry was refined using an automated algorithm to match found and

© 2016 Nature America, Inc. All rights reserved.

predicted peaks to subpixel accuracy[6]. Filters were applied that excluded frames with partial Bragg spot-intensity measurements that failed to match a reference set of full measurements with a Pearson correlation coefficient of at least 0.1. Frames were also excluded if they indexed in the wrong Bravais group, had outlying unit cell dimensions or had very low signal, which left 37,487 frames in the final data set. This set of indexed patterns was post-refined and merged into a final data set[36] (overall CC* = 94.0%; 2.25-Å cutoff) for further analysis ($P6_122$, unit cell: a = b = 93.8 Å, c = 132.2 Å; $\alpha = \beta = 90°$, $\gamma = 120°$). The resolution cutoff was estimated as 2.25 Å using a combination of CC*[35] and other refinement parameters. The final data set had an overall R_{split} = 9.4% and CC* = 0.16 in the highest resolution shell.

Refinement of 30S ribosomal subunit structure. We determined the ambient-temperature 30S-paromomycin structure using the automated molecular replacement program Phaser[37] with the previously published cryo-cooled 30S ribosomal subunit–paromomycin complex synchrotron structure as a search model (PDB ID 4DR2)[14]. The resulting structure was refined with rRNA modifications, which are mostly located near the decoding center at which paromomycin binds. This choice of starting search model minimized experimental variations between the two structures such as sample preparation, crystal growth, model registry and data processing. Coordinates of the 4DR2 with additional RNA and protein modifications were used for initial rigid body refinement with the PHENIX[38] software package. During initial refinement of the ambient-temperature XFEL structure, the entire 16S rRNA h28 hinge 1 region was omitted and the new h28 model was built into unbiased difference density using RCrane[39]. After simulated-annealing refinement, individual coordinates, three group B factors per residue and TLS parameters were refined. Potential positions of magnesium and potassium ions were compared with those in a high-resolution (2.5 Å) 30S subunit structure (PDB ID 2VQE)[40] in the program COOT[41], and positions with strong difference densities were retained. All magnesium atoms were replaced with magnesium hexahydrate. Water molecules located outside of areas of significant electron density were manually removed. The Ramachandran statistics (most favored, additionally allowed, generously allowed and disallowed) were 90.4%, 8.2%, 1.3% and 0.1%, respectively. The structure refinement statistics are summarized in **Supplementary Table 2**. Structure alignments were performed using the alignment algorithm of PyMOL (http://www.schrodinger.com/pymol) with the default 2σ rejection criterion and five iterative alignment cycles. Alignments used to detect repositioning of the 30S subunit h28 in both crystal structures were performed using 16S rRNA phosphate atoms from residues 5–1,532. All X-ray crystal structure figures were produced with PyMOL.

Thermolysin structure refinement. We determined the thermolysin structure using the program Phaser[37] by using the previously published SFX structure as a search model (PDB ID 4OW3)[6]. Coordinates of 4OW3 were used for initial rigid-body refinement with the PHENIX[38] software package followed by individual coordinates, three group B factors per residue and TLS parameter refinement. Potential positions of water molecules were compared with those in a high-resolution (1.8 Å) thermolysin SFX structure (PDB ID 4TNL)[26] in COOT[41], and positions with strong difference densities were retained. The Ramachandran statistics (most favored, additionally allowed, generously allowed and disallowed) were 93.0%, 5.9%, 1.1% and 0.0%, respectively. The structure refinement statistics are summarized in **Supplementary Table 2**. All X-ray crystal structure figures were produced with PyMOL.

21. Oshima, T. & Imahori, K. *J. Biochem.* **75**, 179–183 (1974).
22. DeMirci, H. *et al. RNA* **16**, 2319–2324 (2010).
23. Wimberly, B.T. *et al. Nature* **407**, 327–339 (2000).
24. Ibrahim, M. *et al. Struct. Dyn.* **2**, 041705 (2015).
25. Kern, J. *et al. Biochim. Biophys. Acta* **1706**, 147–157 (2005).
26. Kern, J. *et al. Nat. Commun.* **5**, 4371 (2014).
27. Kern, J. *et al. Proc. Natl. Acad. Sci. USA* **109**, 9721–9726 (2012).
28. Kern, J. *et al. Science* **340**, 491–495 (2013).
29. Kameshima, T. *et al. Rev. Sci. Instrum.* **85**, 033110 (2014).
30. White, T.A. *et al. J. Appl. Crystallogr.* **45**, 335–341 (2012).
31. Barty, A. *et al. J. Appl. Crystallogr.* **47**, 1118–1131 (2014).
32. Yefanov, O. *et al. Opt. Express* **23**, 28459–28470 (2015).
33. Kirian, R.A. *et al. Opt. Express* **18**, 5713–5723 (2010).
34. White, T.A. *et al. Acta Crystallogr. D Biol. Crystallogr.* **69**, 1231–1240 (2013).
35. Karplus, P.A. & Diederichs, K. *Science* **336**, 1030–1033 (2012).
36. Sauter, N.K. *J. Synchrotron Radiat.* **22**, 239–248 (2015).
37. McCoy, A.J. *et al. J. Appl. Crystallogr.* **40**, 658–674 (2007).
38. Adams, P.D. *et al. Acta Crystallogr. D Biol. Crystallogr.* **66**, 213–221 (2010).
39. Keating, K.S. & Pyle, A.M. *Acta Crystallogr. D Biol. Crystallogr.* **68**, 985–995 (2012).
40. Kurata, S. *et al. J. Biol. Chem.* **283**, 18801–18811 (2008).
41. Emsley, P., Lohkamp, B., Scott, W.G. & Cowtan, K. *Acta Crystallogr. D Biol. Crystallogr.* **66**, 486–501 (2010).

© 2016 Nature America, Inc. All rights reserved.

doi:10.1038/nmeth.3667